Electronic Supplementary Material (ESI) for Chemical Communications.

Supporting Information

Cove-region O-annulation of arylene diimide enables ambipolar transporting polycyclic aromatic hydrocarbon with strong NIR absorption

Kaihua Zhang,‡[a] Jing Guo,‡[a] Hao Liu,[a] Xiaofeng Wang,[a] Yifan Yao,[a] Kun Yang,[a] Zebing Zeng*[a]

[a] Shenzhen Research Institute of Hunan University, Shenzhen 518000, State Key Laboratory of Chemo/Biosensing and Chemometrics, College of Chemistry and Chemical Engineering, Hunan University, Changsha 410082, P. R. China.
E-mail: zbzeng@hnu.edu.cn

Content

1. **General Methods** **S2**
2. **Synthetic Details** **S2**
3. **Theoretical Calculations of ADA and *O*-ADA** **S8**
4. **Additional UV-*vis*-NIR Absorption Spectra** **S11**
5. **OFETs Device Fabrication and Characterization** **S11**
6. **Photothermal Effect and PCE Calculation** **S13**

1. General Methods

Solvents were purified and dried by standard methods prior to use. All commercially available reagents were used without further purification unless otherwise noted. Column chromatography was generally performed on silica gel (200 - 300 mesh) and reactions were monitored by thin layer chromatography (TLC) using silica gel GF254 plates with UV light to visualize the course of reaction. ^{1}H NMR and ^{13}C NMR data were recorded on a 400 MHz or 100 MHz spectrometer using $CDCl_3$ as solvent at room temperature. The chemical shifts (δ) are reported in ppm and coupling constants (*J*) in Hz. ^{1}H NMR chemical shifts were referenced to $CDCl_3$ (7.26 ppm) and THF-d_8. (3.58 ppm and 1.73 ppm). ^{13}C NMR chemical shifts were referenced to $CDCl_3$ (77.00 ppm) and THF-d_8. (67.40 ppm and 25.38 ppm). The following abbreviations were used to explain the multiplicities: s = singlet, d = doublet, t = triplet, m = multiplet. Cyclic voltammetry (CV) was performed on a Chenhua 650D electrochemical using a three-electrode cell with a glassy carbon working electrode, a platinum wire counter electrode, and an $Ag/AgNO_3$ or Ag/AgCl reference electrode in anhydrous solvents containing recrystallized tetra-*n*-butyl-ammoniumhexafluorophosphate ($TBAPF_6$, 0.1 M) as supporting electrolyte at 298 K. The potential was externally calibrated against the ferrocene/ferrocenium couple. Steady-state UV-*vis*-NIR absorption spectra were recorded on a Shimadzu UV-3600 plus spectrometer. HR MALDI-TOF mass spectra recorded on Finnigan MAT TSQ 7000 instrument. Photothermal conversion behavior recorded by FLIR-1910581 thermal camera.

2. Synthetic Details

Synthesis of Compound 1b

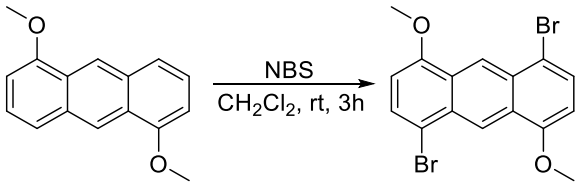

1b

A solution of 1,5-dimethoxyanthracene[1] (2.38 g, 10 mmol, 1.0 equiv.) in anhydrous CH_2Cl_2 (200 mL) was cooled to 0 °C under an argon atmosphere. NBS (3.56 g, 20 mmol, 2.0 equiv.) was added in small portions over a 30 min period at 0 °C. After the addition, the temperature was slowly allowed to rise to r.t. and the mixture was stirred for additional 3 hours. After the reaction was completed, the product was separated in the reaction flask and filtered to obtain a yellow solid (3.64 g, 92%) without further purification. ^{1}H NMR (400 MHz, $CDCl_3$): δ 9.14 (s, 2H), 7.70 (d, *J* = 7.6 Hz, 2H), 6.66 (d, *J* = 7.5 Hz, 2H), 4.09 (s, 6H). ^{13}C NMR (100 MHz, $CDCl_3$) δ 155.2, 130.2, 126.4, 121.6, 103.1, 55.8. MS (MALDI-TOF, m/z): caldc for $C_{16}H_{12}Br_2O_2$ $[M]^+$, 395.9184; found 395.9175, (error = −2.2 ppm).

Synthesis of Compound 2a

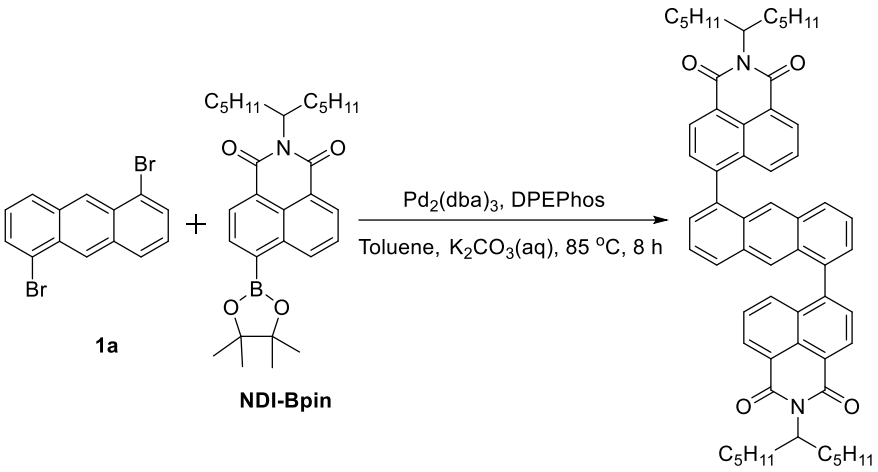

A mixture of 1,5-dibromoanthracene[2] (336 mg, 1 mmol) and NDI-Bpin[3] (1.192 g, 2.5 mmol) and aqueous solution of K_2CO_3 (252 mg in 1 mL), EtOH (5 ml) and Toluene (50 mL) was Argon bubbled to degas the oxygen for 30 min. $Pd_2(dba)_3$ (91.5 mg, 0.1 mmol) and DPEphos (161 mg, 0.3 mmol) was then added and heated up to 85 °C for 8 h under Argon atmosphere. Upon completion, the mixture was cooled down to room temperature and diluted with CH_2Cl_2 (30 mL) and water (10 mL). After removal of the solvents, the residue was purified by silica gel chromatography (petroleum ether/dichloromethane = 2/1) to afford compound **2a** (675 mg, 77%) as a pale yellow solid. ^{1}H NMR (400 MHz, $CDCl_3$): δ 8.78 (d, *J* = 6.8 Hz, 2H), 8.64 (d, *J* = 7.1 Hz, 2H), 8.03 (d, *J* = 7.4 Hz, 2H), 7.80 – 7.87 (m, 6H), 7.46-7.60 (m, 6H), 5.27 (m, 2H), 2.31 (m, 4H), 1.89 (m, 4H), 1.33 (m, 24H), 0.87 (m, 12H). ^{13}C NMR (100 MHz, $CDCl_3$) δ 165.26, 163.22, 144.55, 136.27, 132.47, 131.85, 131.82, 131.27, 130.81, 130.25, 129.43, 129.10, 129.00. 128.71, 128.68, 127.92, 127.00, 125.55, 125.05, 125.01, 55.13, 32.87, 31.82, 26.16, 23.39, 14.61. MS (MALDI-TOF, m/z): caldc for $C_{60}H_{64}N_2O_4$ $[M]^+$, 876.4866, found 876.4855, (error = -1.3 ppm).

Synthesis of Compound 2b

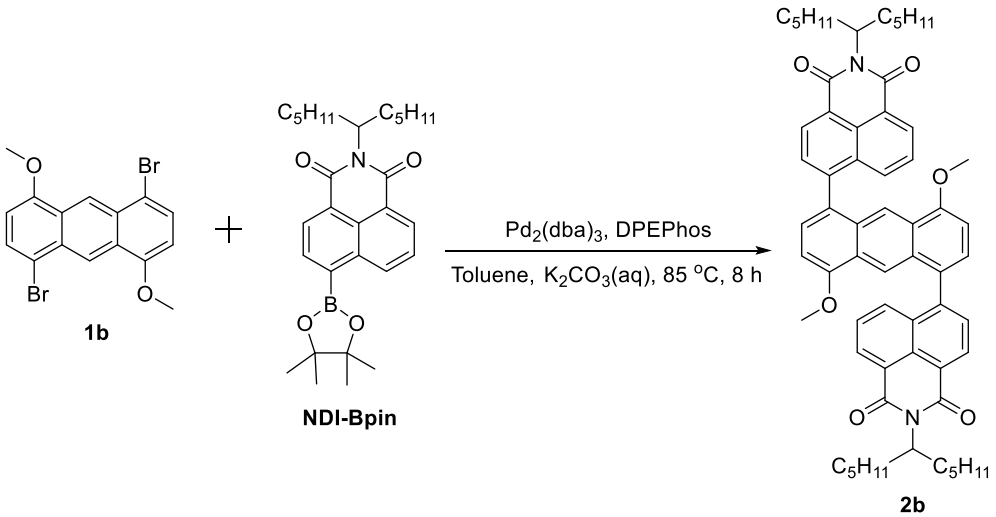

Compound 2b was synthesized in 65% yield as a yellow solid, a similar synthetic process to that of 2a. ^{1}H NMR (400 MHz, $CDCl_3$): δ 8.72 (s, 2H), 8.63 (s, 2H), 8.51 (d, *J* = 8.0 Hz, 2H), 7.96 (m, 2H), 7.89 (d, *J* = 7.4 Hz, 2H), 7.59 (m, 2H), 7.36 (d, *J* = 7.6 Hz, 2H), 6.83 (d, *J* = 7.7 Hz, 2H), 5.29 – 5.22 (m, 2H), 3.91 (s, 6H), 2.32 (m, 4H), 1.85 (m, 4H), 1.32 (m, 24H), 0.85 (m, 12H). ^{13}C NMR (100 MHz, $CDCl_3$) δ 165.27, 164.16, 155.82, 145.29, 132.70, 131.68, 131.03, 129.54, 129.44, 128.89, 128.87, 128.30, 128.27, 126.72, 125.24, 123.49, 122.80, 122.72, 121.89, 119.68, 101.79, 55.56, 54.07, 32.42, 31.81, 27.21, 22.13, 14.07. MS (MALDI-TOF, m/z): caldc for $C_{62}H_{68}N_2O_6$ $[M]^+$, 936.5077, found 936.5076, (error = 0.1 ppm).

Synthesis of Compound 3

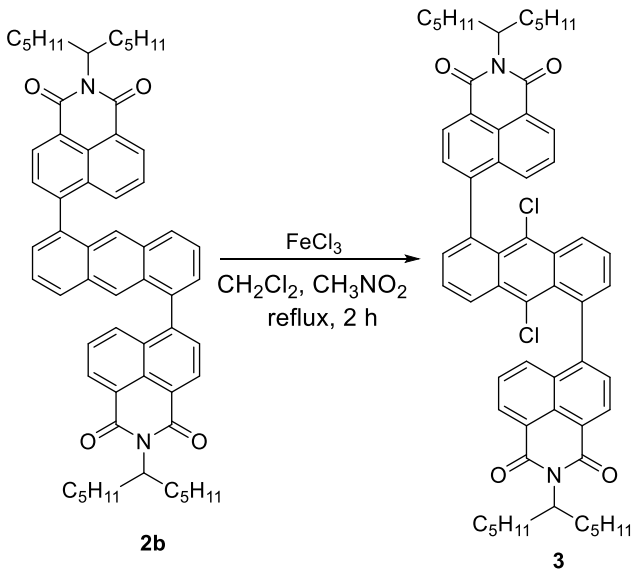

To a solution of compound **2b** (184 mg, 0.21 mmol) in CH_2Cl_2 (100 mL) under Argon atmosphere in an ice bath, anhydrous $FeCl_3$ (680 mg, 4.2 mmol) dissolve in CH_3NO_2 (3 mL) was slowly added. The mixture was then heated up to the 50 °C and stirred for 2 h. Upon reaction completion, the reaction was quenched by H_2O (15 mL). The organic layer was collected, and the remaining aqueous solution was further extracted by dichloromethane. After removing the organic solvents under reduced pressure, the residue was purified by silica gel chromatography (petroleum ether/dichloromethane = 2/1) to afford compound **3** (149 mg, 75%) as a yellow solid. ^{1}H NMR (400 MHz, $CDCl_3$): δ 8.62 (d, *J* = 9.6 Hz, 6H), 7.87 (d, *J* = 8.5 Hz, 1H), 7.76 – 7.73 (m, 1H), 7.68 – 7.53 (m, 8H), 5.25 (m, 2H), 2.32 (m, 4H), 1.94 (m, 4H), 1.41 (m, 24H), 0.91 (m, 12H). ^{13}C NMR (100 MHz, $CDCl_3$) δ 165.54, 165.28, 145.96, 135.85, 135.79. 132.82, 131.44, 129.15, 128.53, 127.97, 127.81, 126.94, 126.43, 126.36, 55.47, 32.43, 31.80, 26.68, 22.58, 14.76. MS (MALDI-TOF, m/z): caldc for $C_{60}H_{62}Cl_2N_2O_4$ $[M]^+$, 944.4087, found 944.4085, (error = -0.21 ppm).

Synthesis of Compound ADA

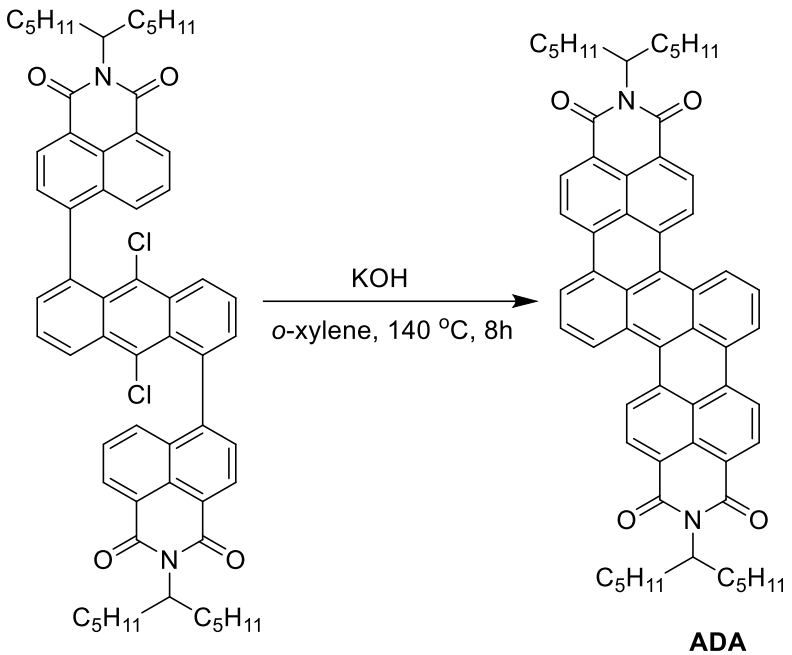

3 **ADA**

To a solution of compound **3** (100 mg, 0.11 mmol) in *o*-xylene (30 mL) under Argon atmosphere, KOH (1.23 g, 22 mmol) was added under argon atmosphere. The reaction mixture was stirred at 140 °C for 8h. To confirm the consumption of starting material, the reaction was monitored by TLC. Upon reaction completion, the mixture was diluted with dichloromethane (40 mL) and water (10 mL), and washed with brine (30 mL). After removal of the solvents, the residue was purified by silica gel chromatography (petroleum ether/dichloromethane = 1/1) to afford compound 7 (83.1 mg, 90%) as a green solid. ^{1}H NMR (400 MHz, $CDCl_3$): δ 8.62 (d, *J* = 8.7 Hz, 6H), 8.52 (m, 4H), 8.24 (d, *J* = 7.9 Hz, 2H), 7.72 (t, *J* = 8.0 Hz, 2H), 5.25 (m, 2H), 2.31 (m, 4H), 1.91 (m, 4H), 1.41 (m, 24H), 0.86 (m, 12H). ^{13}C NMR (100 MHz, $CDCl_3$) δ 164.59, 164.31, 163.60, 163.09, 134.57, 134.16, 130.72, 130.00, 128.85, 128.26, 128.05, 127.55, 126.41, 124.30, 123.40, 121.70, 120.95, 120.42, 53.81, 32.32, 31.33, 26.78, 22.66, 14.10. MS (MALDI-TOF, m/z): caldc for $C_{60}H_{60}N_2O_4$ $[M]^+$, 872.4553, found 872.4558, (error = 0.53 ppm).

Synthesis of Compound 4

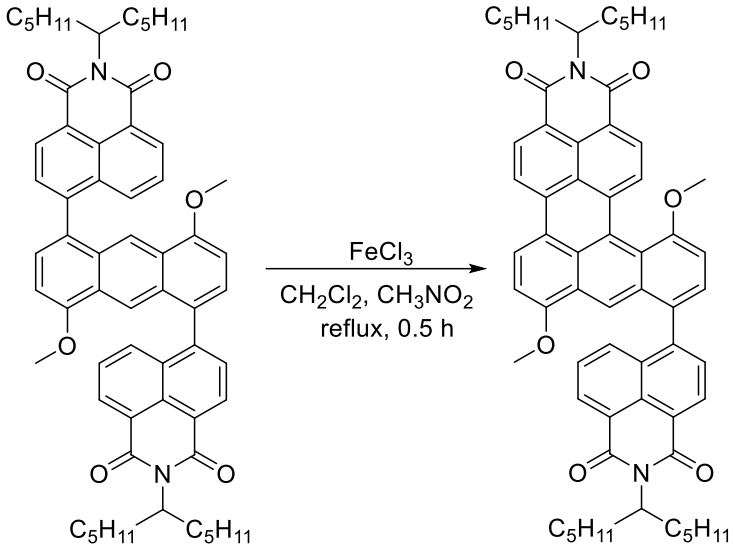

2b **4**

To a solution of compound **2b** (200 mg, 0.21 mmol) in CH_2Cl_2 (100 mL) under Argon atmosphere in an ice bath, anhydrous $FeCl_3$ (680 mg, 4.2 mmol) soluted in CH_3NO_2 (3 mL) was slowly added.[4] The mixture was then heated up to the 50 °C and stirred for 0.5 h. Upon reaction completion, the reaction was quenched by H_2O (15 mL). The organic layer was collected, and the remaining aqueous solution was further extracted by dichloromethane. After removing the organic solvents under reduced pressure, the residue was purified by silica gel chromatography (petroleum ether/dichloromethane = 1/2) to afford compound **4** (163 mg, 82%) as a purple solid. ^{1}H NMR (400 MHz, $CDCl_3/CS_2$ = 5/1): δ 9.46 (s, 2H), 8.25 (s, 2H), 7.87 (s, 2H), 7.29 (m, 3H), 7.24 (m, 3H), 6.24 (d, *J* = 6.6 Hz, 2H), 5.28 – 5.21 (m, 2H), 4.13 (s, 6H), 2.38 (m, 4H), 2.02 (m, 4H), 1.47 (m, 24H), 0.98 (m, 12H). ^{13}C NMR (100 MHz, $CDCl_3/CS_2$ = 5/1) δ 165.73, 165.25, 164.67, 155.87, 155.50, 147.39, 132.81, 131.78, 131.13, 129.64, 129.54, 128.98, 128.85, 128.39, 127.72, 127.60, 126.81, 125.35, 124.08, 123.32, 123.17, 122.09, 119.78, 118.31, 101.76, 101.02, 56.91, 55.91, 54.92, 32.81, 32.21, 27.08, 22.33, 14.12. MS (MALDI-TOF, m/z): caldc for $C_{62}H_{66}N_2O_6$ $[M]^+$, 934.4921, found 934.4899, (error = -2.4 ppm).

Synthesis of Compound *O*-ADA

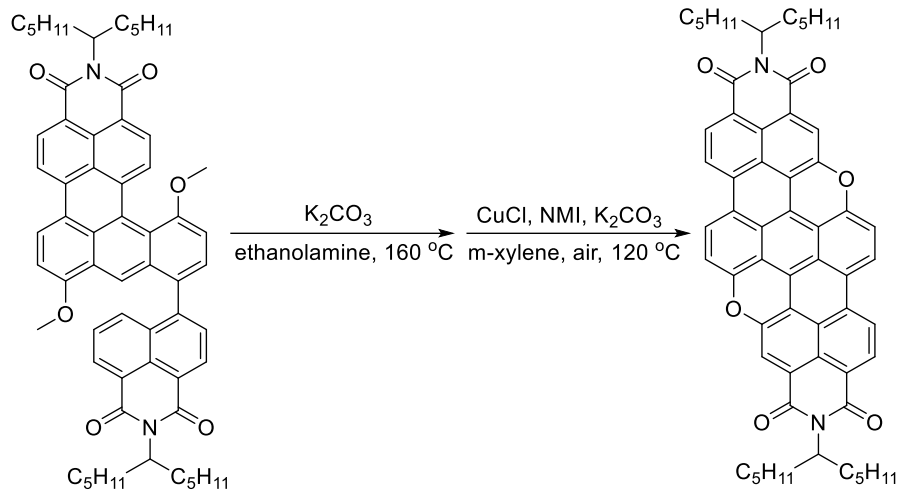

To a solution of compound **4** (200 mg, 0.21 mmol) in ethanolamine (15 mL), K_2CO_3 (2 g, 14.5 mmol) were added under an argon atmosphere. The reaction mixture was stirred at 145 ℃ for 6h and continued 160 °C for overnight. To confirm the consumption of starting material, the reaction was monitored by TLC. Upon reaction completion, the mixture was diluted with dichloromethane and filterd out the residue. The solvent was removed under vacuum and then the intermediate product used directly for the next reaction, which was soluted in 20mL m-xylene. To this mixture, CuCl (6.5 mg, 0.07 mmol), NMI (11 mg, 0.13 mmol), K_2CO_3 (110 mg, 0.88 mmol) were added in air The reaction mixture was stirred at 120 °C.[5] To confirm the consumption of starting material, the reaction was monitored by TLC. Upon reaction completion, the mixture was diluted with methylene dichloride (20 mL) and filterd out the residue. After removal of the solvents, the residue was purified by silica gel chromatography (petroleum ether/ tetrahydrofuran = 4/1) to afford compound ***O*-ADA** (48.2 mg, 25%) as a brown solid. ^{1}H NMR (400 MHz, THF-d_8/CS_2 = 5/1): δ 8.69 (d, *J* = 9.2 Hz, 2H), 8.18 (d, *J* = 6.2 Hz, 2H), 7.65 (s, 2H), 7.01 (d, *J* = 7.0 Hz, 2H), 6.38 (d, *J* = 7.4 Hz, 2H), 5.29 (m, 2H), 2.36 (m, 4H), 1.90 (m, 4H), 1.39 (m, 24H), 0.92 (m, 12H). ^{13}C NMR (100 MHz, THF-d_8/CS_2 = 5/1) δ 168.30, 155.92, 150.11, 132.66, 132.20, 131.47, 129.83, 129.73, 129.32, 128.92, 128.48, 127.14, 125.69, 124.08, 123.61, 54.18, 32.84, 32.42, 27.10, 22.82, 14.73.

3. Theoretical Calculations of ADA and *O*-ADA

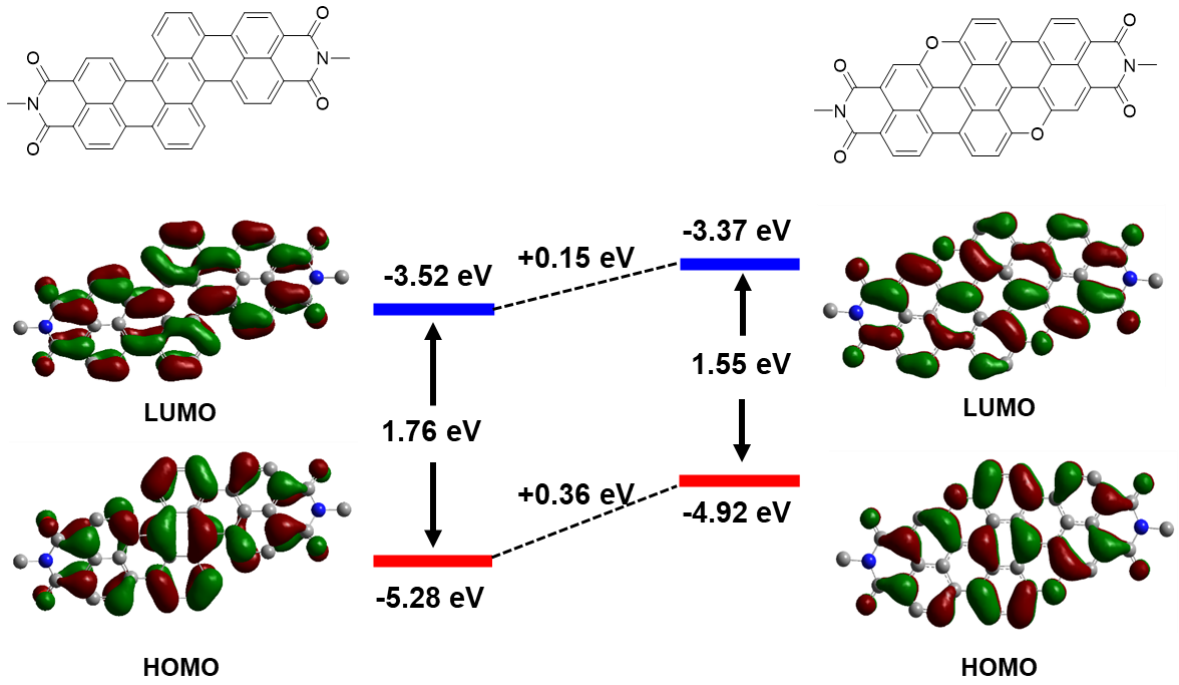

Fig. S1 Calculated MOs profiles of **ADA** and ***O*-ADA** at the B3LYP/6-31G(d, p) level.

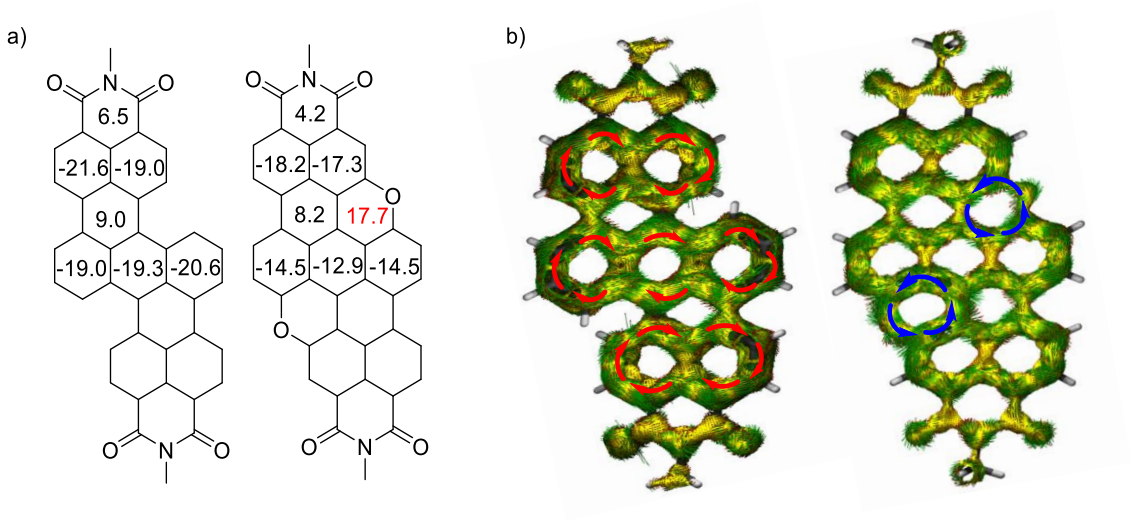

Fig. S2 DFT-calculated (a) NICS(1)$_{ZZ}$ values and (b) ACID plots of **ADA** and ***O*-ADA** at the B3LYP/6-31G(d,p) level.

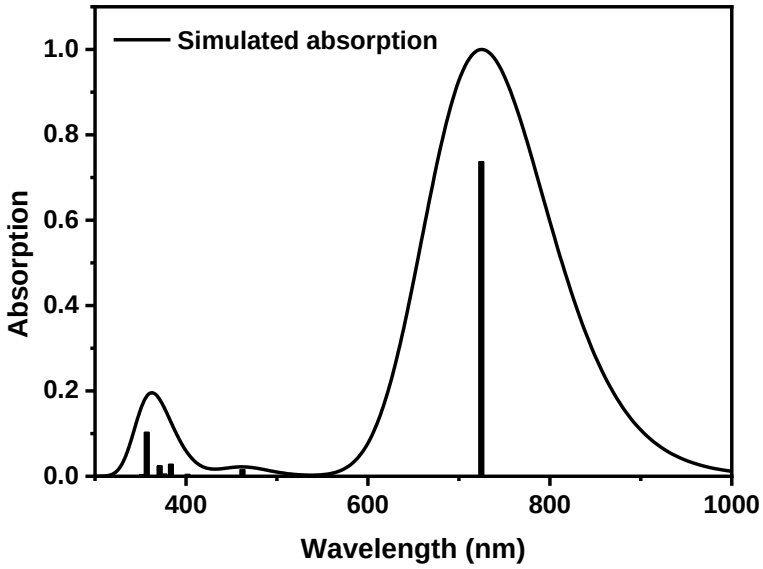

Fig. S3 Simulated absorption spectrum of **ADA** calculated at the B3LYP/6-31G (d, p) level.

Table S1 Major transitions of **ADA** calculated by TD-DFT.

Excited state	Wavelength(nm)	Osc. Strength	Description
1	724.71	0.8043	HOMO->LUMO (102%)
2	541.68	0.0005	H-1->LUMO (39%), HOMO->L+1 (61%)
3	462.06	0.0174	H-1->LUMO (58%), HOMO->L+1 (37%)
4	408.06	0.0002	H-2->LUMO (93%)
5	407.86	0.0001	H-3->LUMO (93%)
6	401.63	0.0048	H-6->LUMO (22%), H-4->LUMO (61%)
7	383.31	0.0307	H-7->LUMO (20%), HOMO->L+2 (67%)
8	379.32	0.0011	H-11->LUMO (10%), H-6->LUMO (34%), HOMO->L+3 (32%)
9	378.62	0.0016	H-5->LUMO (84%)
10	376.27	0.0057	H-9->LUMO (11%), H-6->LUMO (31%), H-4->LUMO (16%), HOMO->L+3 (32%)
11	375.60	0.0011	H-8->LUMO (81%)
12	371.03	0.0269	H-9->LUMO (19%), H-7->LUMO (42%), HOMO->L+3 (17%), HOMO->L+5 (15%)
13	356.79	0.1127	H-1->L+1 (68%), HOMO->L+5 (19%)
14	356.47	0.0012	H-10->LUMO (59%), HOMO->L+4 (23%)

15	351.55	0.0046	H-12->LUMO (12%), H-10->LUMO (13%), HOMO->L+4 (64%)

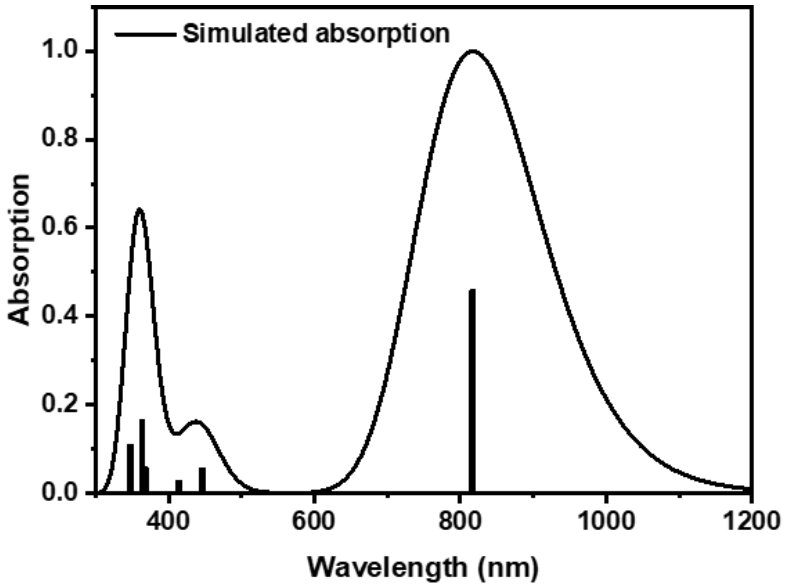

Fig. S4 Simulated absorption spectrum of ***O*-ADA** calculated at the B3LYP/6-31G (d, p) level.

Table S2 Major transitions of ***O*-ADA** calculated by TD-DFT.

Excited state	Wavelength(nm)	Osc. Strength	Description
1	816.55	0.6261	HOMO->LUMO (102%)
2	669.82	0	HOMO->L+1 (96%)
3	449.30	0	H-1->LUMO (91%)
4	445.79	0.0773	HOMO->L+2 (85%), HOMO->L+3 (10%)
5	439.32	0.0038	HOMO->L+2 (12%), HOMO->L+3 (42%), HOMO->L+4 (43%)
6	414.37	0.0391	HOMO->L+3 (45%), HOMO->L+4 (48%)
7	401.23	0	H-2->LUMO (12%), HOMO->L+5 (85%)
8	389.75	0	H-2->LUMO (79%)
9	389.29	0	H-3->LUMO (80%)
10	389.29	0.0001	H-4->LUMO (80%)
11	368.61	0.0793	H-5->LUMO (88%)
12	363.81	0.2251	H-1->L+1 (78%)
13	347.67	0.1491	H-6->LUMO (70%), H-1->L+1 (12%)

14	347.61	0	H-10->LUMO (10%), H-7->LUMO (19%), HOMO->L+6 (64%)
15	339.29	0.0037	H-9->LUMO (15%), H-8->LUMO (16%), HOMO->L+7 (47%)

4. Additional UV-*vis*-NIR Absorption Spectra

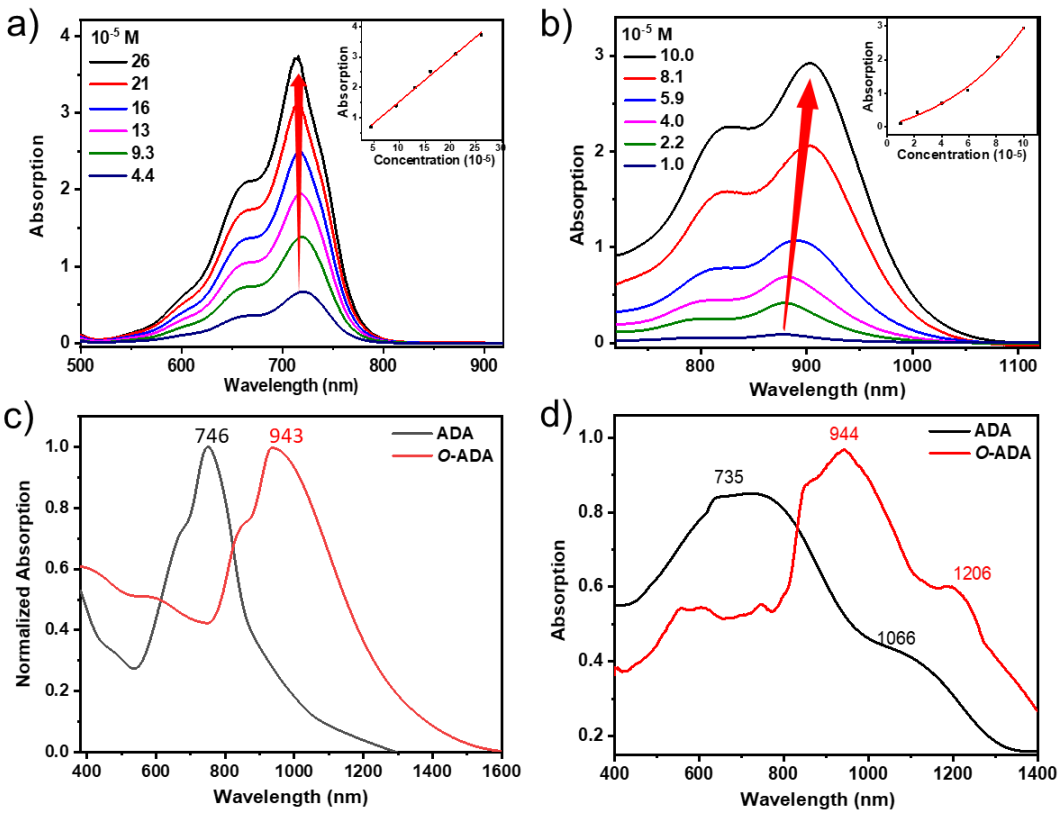

Fig. S5 (a, b) Long wavelength region of concentration-dependent absorption spectra recorded in CH_2Cl_2 solution of **ADA** and ***O*-ADA** at room temperature; (c) UV-*vis*-NIR absorption spectra (400-1600 nm) of **ADA** and ***O*-ADA** in film; (d) UV-*vis*-NIR absorption spectra (400-1400 nm) of **ADA** and ***O*-ADA** in power.

5. OFETs Device Fabrication and Characterization

Bottom-gate/bottom-contact (BG-BC) OFET devices were fabricated using Si/SiO_2 substrates where Si and SiO_2 serve as gate electrode and gate dielectric, respectively. The source and drain gold electrodes with a thickness of 50 nm using 2 nm of chromium as an adhesion layer were prepared by standard lithography procedures. Before the film depositions, silicon wafers were cleaned with ultrapure water, acetone, and isopropanol for 3 times in sequence. Then, it was conducted by oxygen plasma and passivated by trichloro(octadecyl)silane to reduce the surface traps. Lastly, both PAH films were spin-coated from their pre-heated solutions (4 mg/mL in chlorobenzene, heated at 60 °C for overnight under argon protection) at 1800 rpm for 1 min in an argon-filled glovebox, followed by a thermal annealing treatment at 80 °C for ca. 10 min. In ***O*-ADA**-based OFETs, the channel lengths and widths were 40 μm and 1000 μm, respectively, while

those for devices of **ADA** were 10/1000 µm. The charge carrier mobilities of OFETs were calculated in the saturation regime from a plot of the square root of the drain current vs. gate voltage using the following equation:

$$I_{DS} = \frac{WC_i}{2L}\mu(V_G - V_T)^2$$

I_{DS} is the drain source current, C_i is the capacitance per unit area of the gate dielectric (10 nF/cm^2), L is the channel length, W is the channel width, V_T and V_G are the threshold and gate source voltage

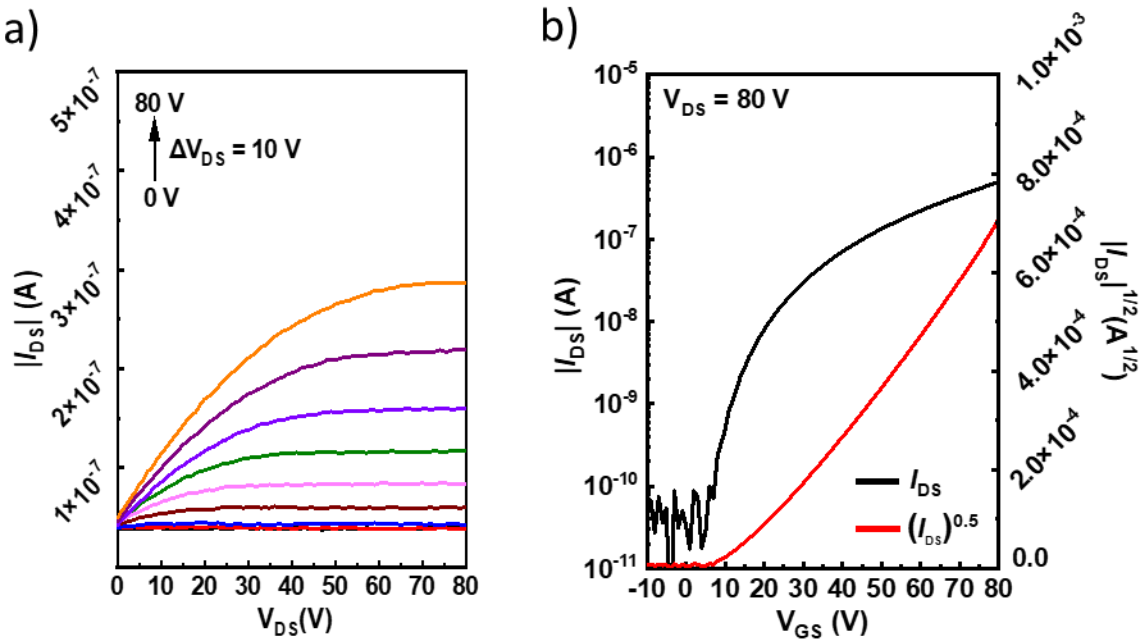

Fig. S6 (a) Output (b) Transfer characteristics of *n*-type mobility of **ADA** based thin-film OFETs.

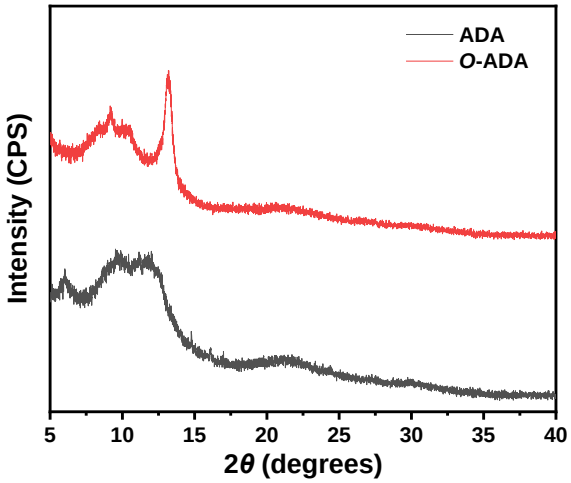

Fig. S7 XRD spectra of **ADA** and ***O*-ADA**.

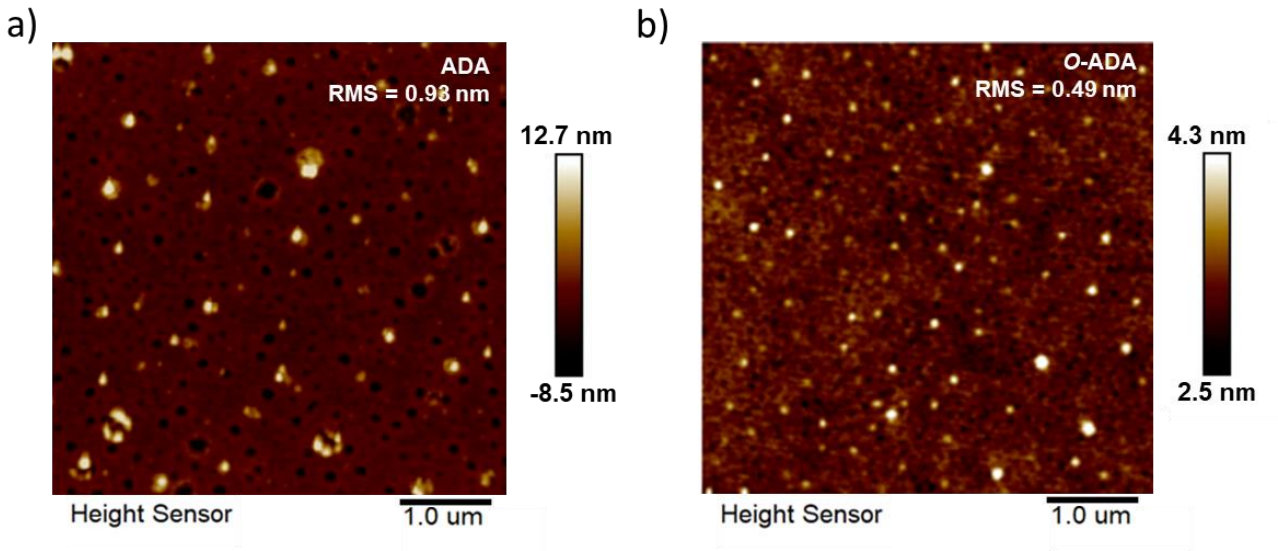

Fig. S8 Tapping-mode AFM image of **ADA** and ***O*-ADA** films.

6. Photothermal Effect and PCE Calculation

For the purpose of evaluating the photothermal ability of **ADA** and ***O*-ADA,** above all, we discussed the effect of power density. **ADA** and ***O*-ADA** solid were irradiated by 808 nm laser at different power densities (0.1, 0.3, 0.5, 0.7 W cm $^{-2}$). The temperature change (ΔT) was recorded by FLIR-1910581 thermal camera. Then, we investigate the effect of concentration on temperature. The photothermal conversion efficiencies (η) were measured according to the reported method:

$$\eta = \frac{hS\Delta T_{max}}{I(1-10^{-A_{808/1064}})}$$

h is the heat transfer coefficient; s is the surface area of the container. I is the laser power and A is the absorbance at 808 nm. ΔT_{max} is the maximum temperature change.

$$\tau_s = \frac{\sum_i m_i C_{p,i}}{hS}$$

mi is the mass of solid; $C_{p,i}$ is the capacity of the carrier (Cpiezoid = 0.8 J/(g•°C)), and τs is the associated time constant.

$$t = -\tau_s \ln \theta$$

ϑ is a dimensionless parameter, known as the driving force temperature.

$$\theta = \frac{T - T_{surr}}{T_{max} - T_{surr}}$$

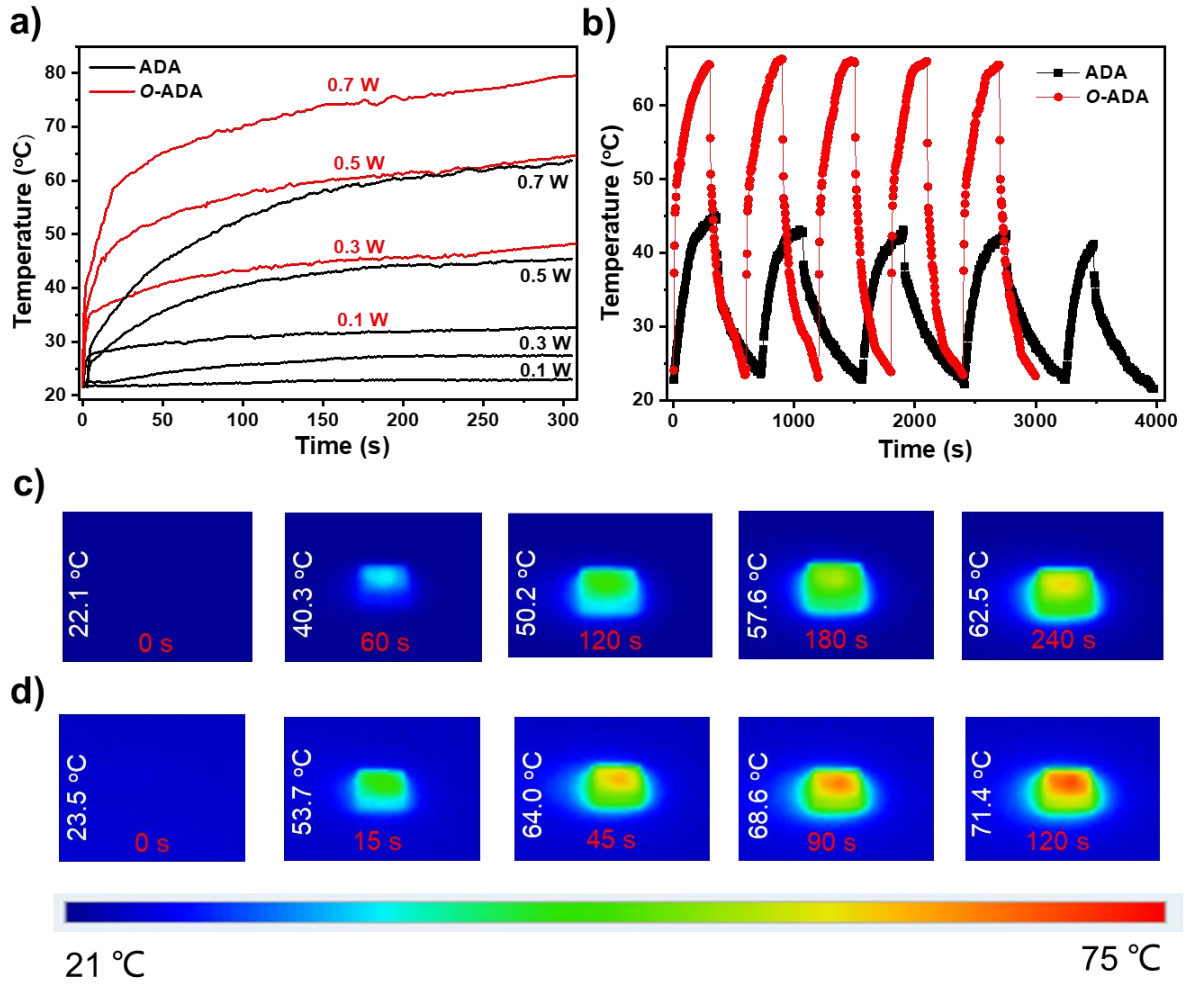

Fig. S9 (a) Photothermal conversion behaviours of **ADA**/***O*-ADA** powders at different power densities (0.1–0.7 W cm^{-2}) under 808 nm light irradiation; (b) photothermal cycle curves of **ADA** and ***O*-ADA** powders at 0.5 W cm^{-2} under 808 nm light irradiation; Thermal images of (c) **ADA** and (d) ***O*-ADA** powders at different time under 808 nm light irradiation.

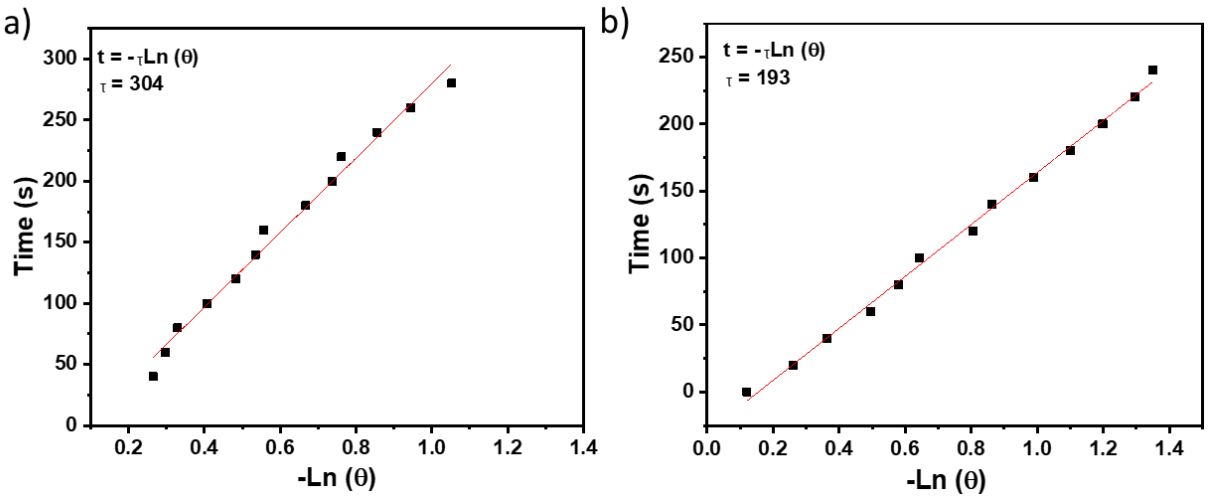

Fig. S10 The time constant for (a) **ADA** (b) ***O*-ADA** calculated with the linear time data from the system cooling period versus the negative natural logarithm of the system driving force temperature.

Table S3. Summary of physical and photoelectronic properties of **ADA** and ***O*-ADA**.

Cmpd	λ_{sol}[a] (nm)	λ_{film}[a] (nm)	λ_{solid}[a] (nm)	E_{HOMO}[b] (eV)	E_{LUMO}[c] (eV)	E_g^{CV}[d] (eV)	E_g^{opt}[e] (eV)	μ_e[f] ($cm^2 V^{-1} s^{-1}$)	μ_h[g] ($cm^2 V^{-1} s^{-1}$)	η[h]
ADA	720	746	735	-5.29	-3.87	1.42	1.54	3.20×10^{-4}	-	21
***O*-ADA**	882	943	944	-5.02	-3.83	1.19	1.12	7.60×10^{-4}	1.07×10^{-3}	35

[a] Absorption maxima. [b] $E_{HOMO} = -4.8\ V - E_{onset}^{ox1}$. [c] $E_{LOMO} = -4.8\ V - E_{onset}^{red1}$. [d] $E_{gap} = E_{LOMO} - E_{HOMO.}$ [e] $E_g^{opt} = 1240/\lambda_{onset.}$ [f] Electron motility. [g] Hole mobility. [h] Photothermal conversion efficiency.

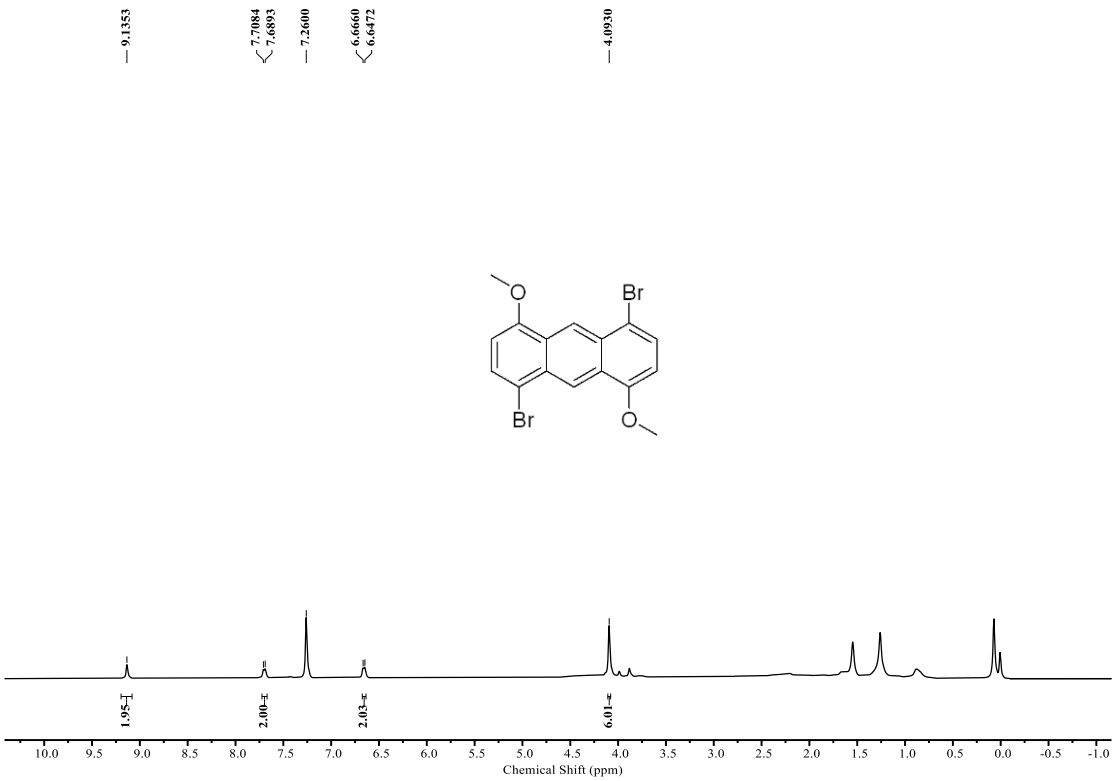

Fig. S11 ^{1}H NMR spectrum (400 MHz) of compound **1b** in $CDCl_3$ at 298 K.

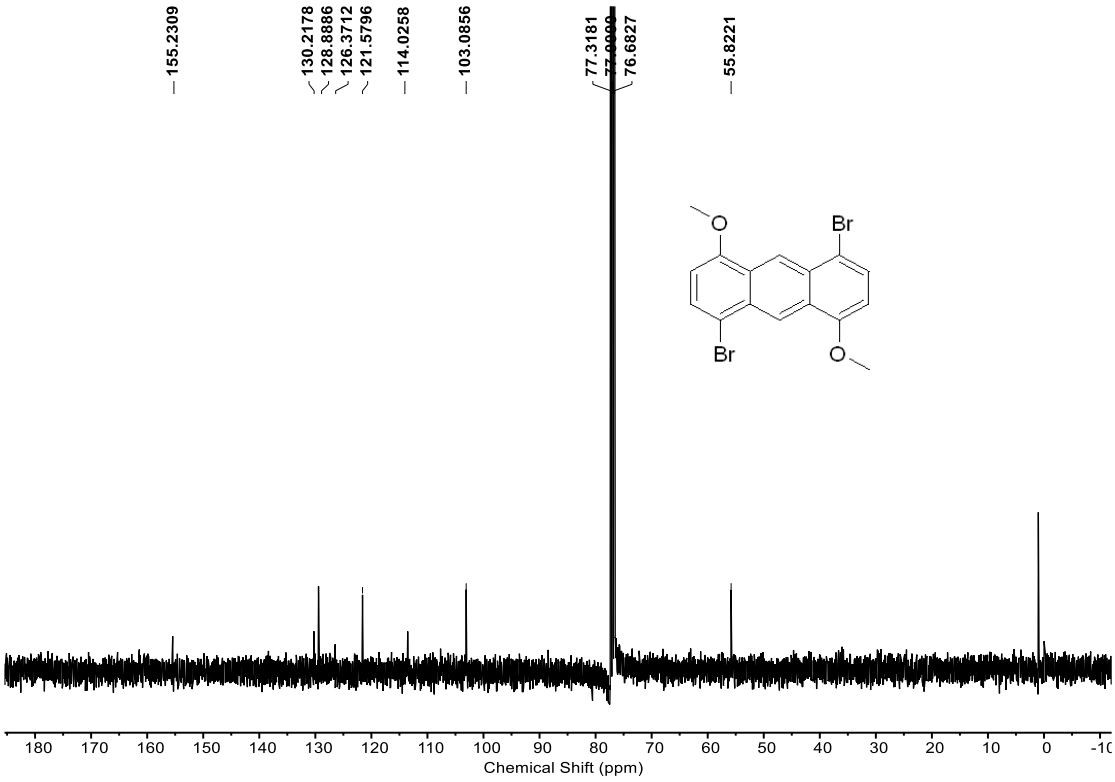

Fig. S12 ^{13}C NMR spectrum (100 MHz) of compound **1b** in $CDCl_3$ at 298 K.

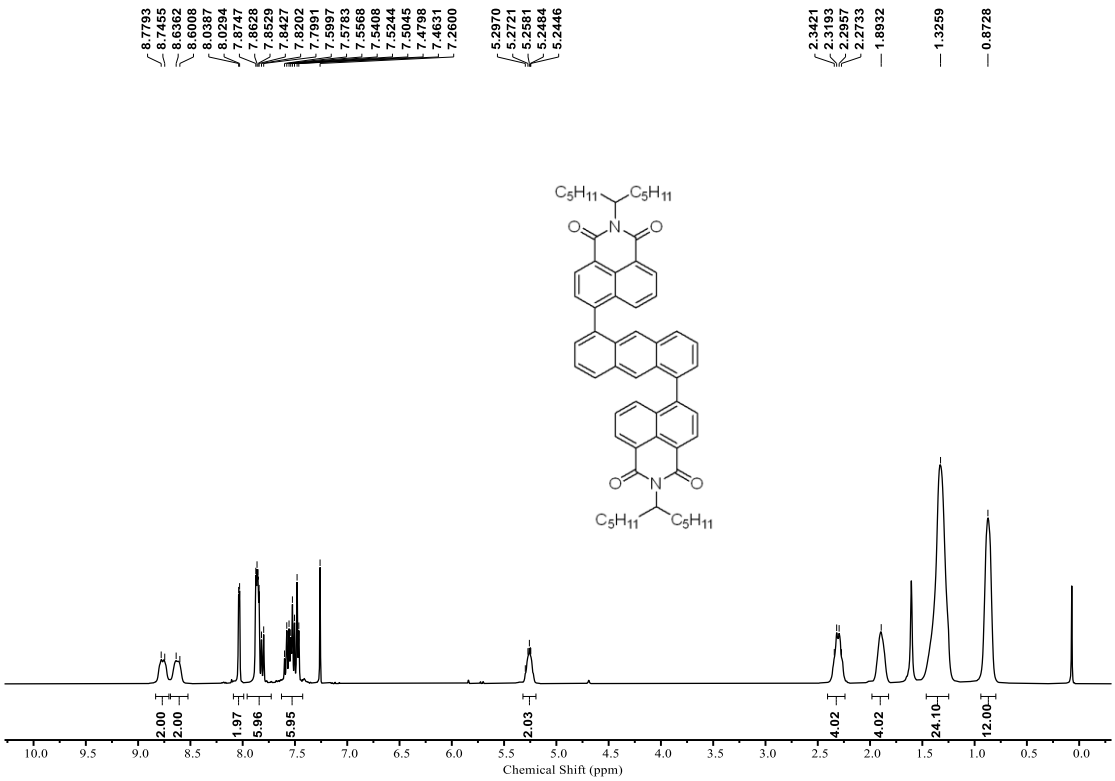

Fig. S13 ^{1}H NMR spectrum (400 MHz) of compound **2a** in $CDCl_3$ at 298 K.

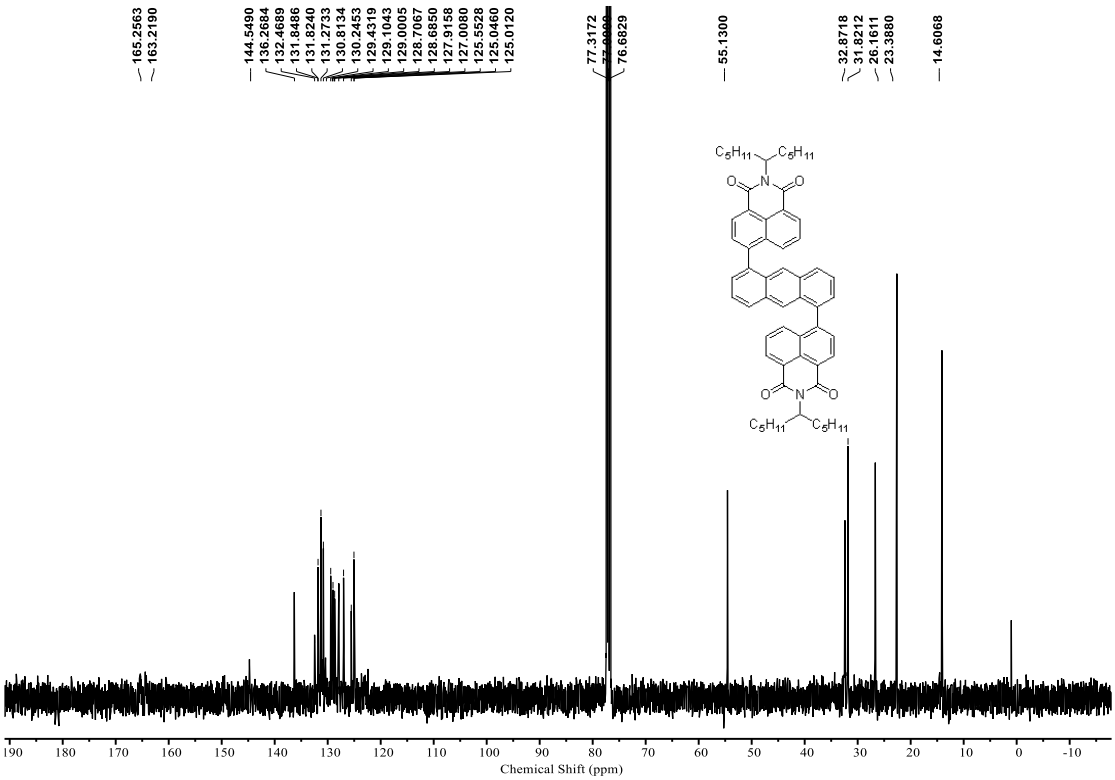

Fig. S14 ^{13}C NMR spectrum (100 MHz) of compound **2a** in $CDCl_3$ at 298 K.

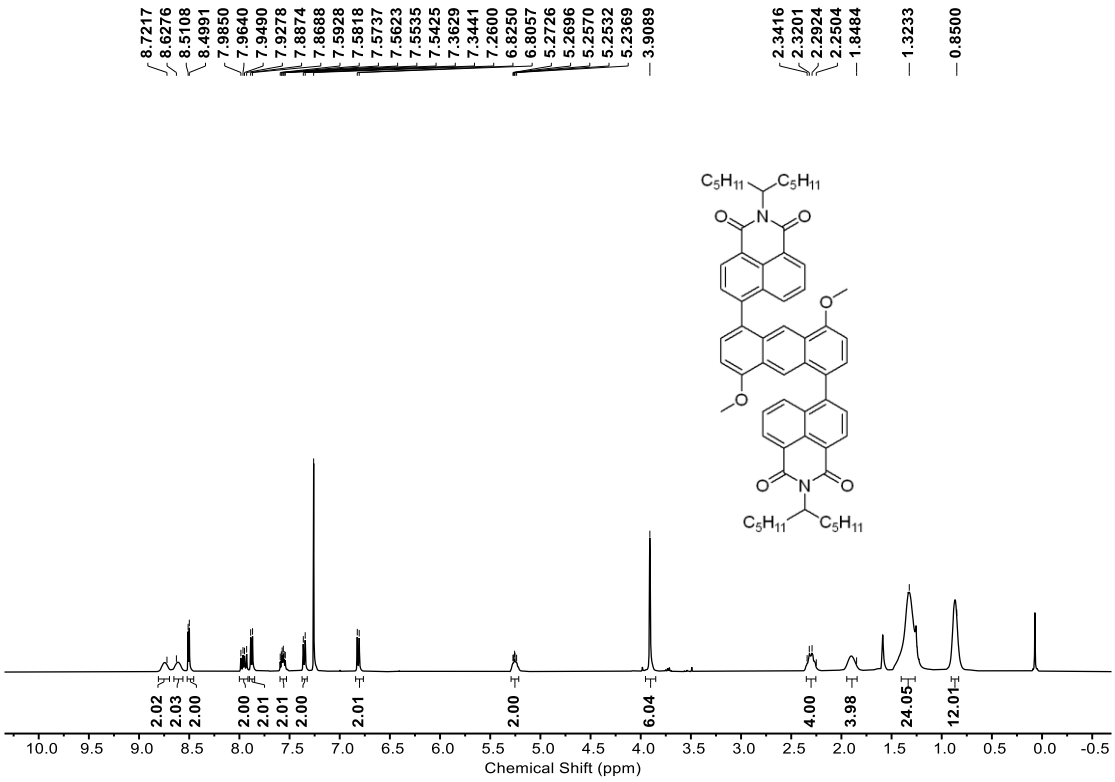

Fig. S15 ^{1}H NMR spectrum (400 MHz) of compound **2b** in $CDCl_3$ at 298 K.

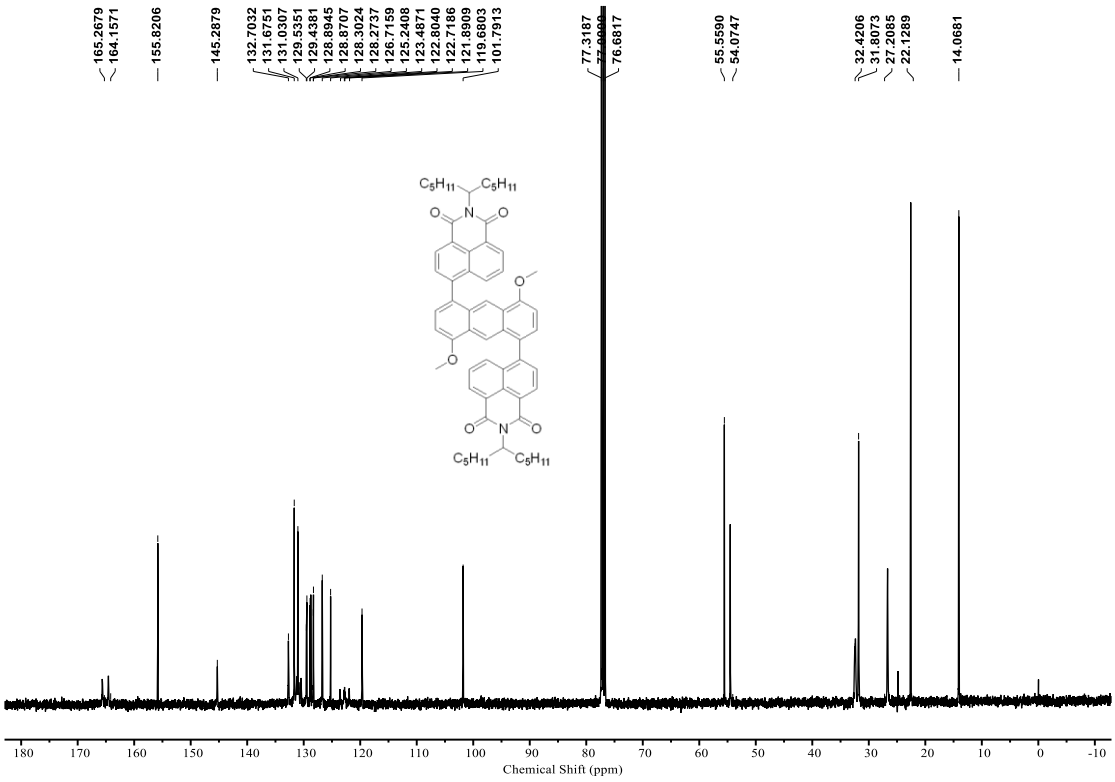

Fig. S16 ^{13}C NMR spectrum (100 MHz) of compound **2b** in $CDCl_3$ at 298 K.

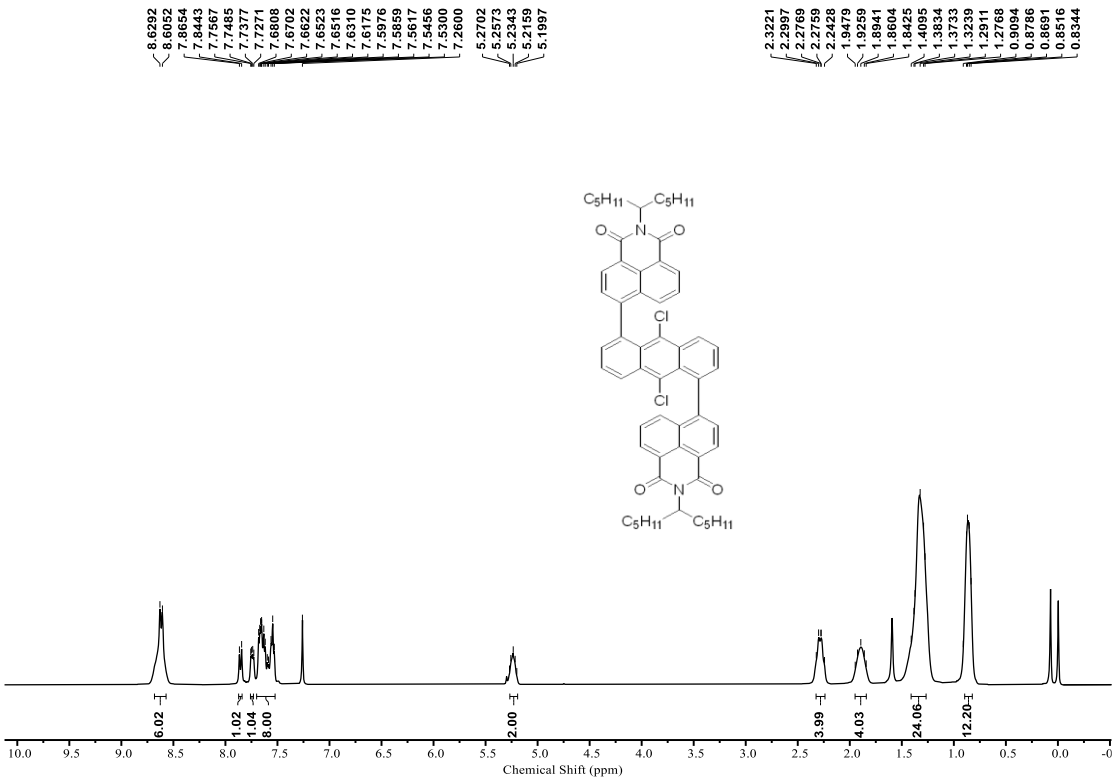

Fig. S17 ^{1}H NMR spectrum (400 MHz) of compound **3** in $CDCl_3$ at 298 K.

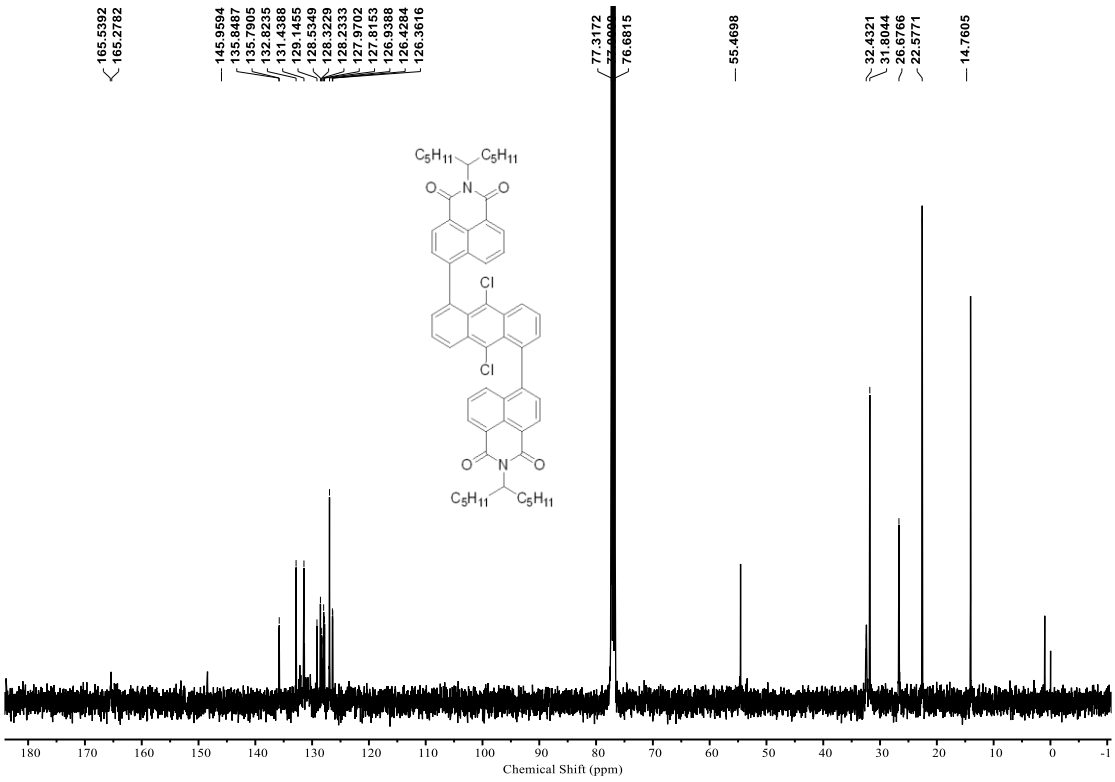

Fig. S18 ^{13}C NMR spectrum (100 MHz) of compound **3** in $CDCl_3$ at 298 K.

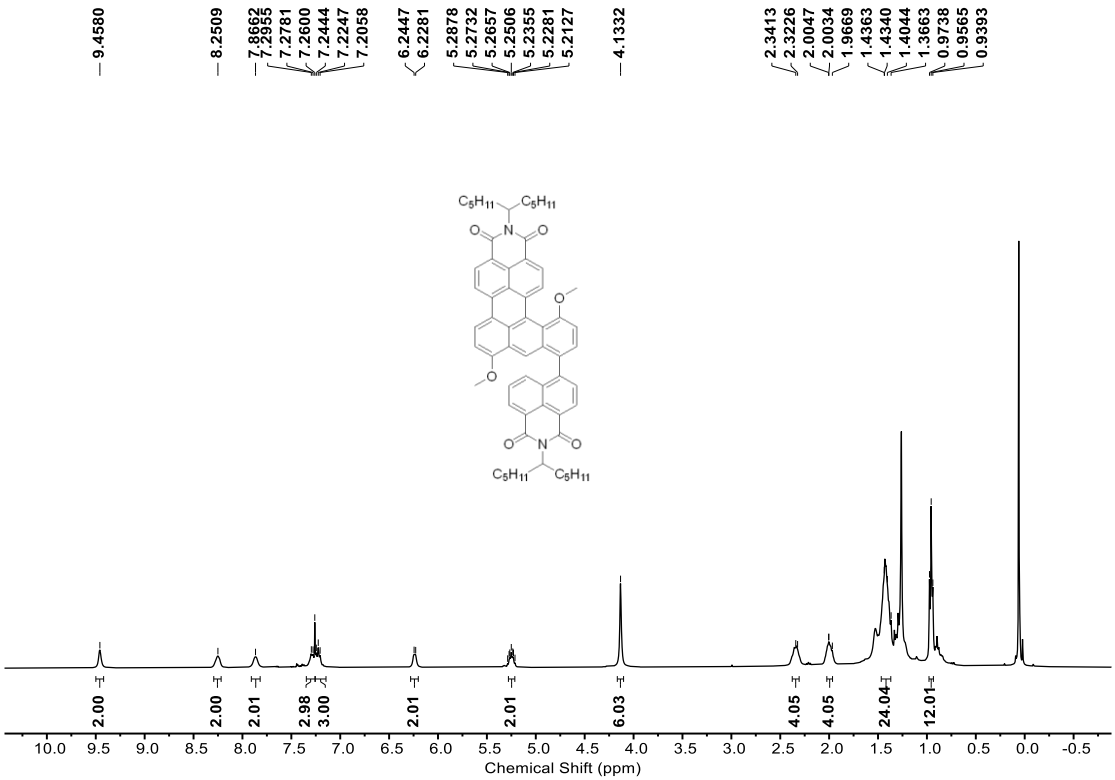

Fig. S19 ^{1}H NMR spectrum (400 MHz) of compound **4** in $CDCl_3/CS_2$ (5/1) at 298 K.

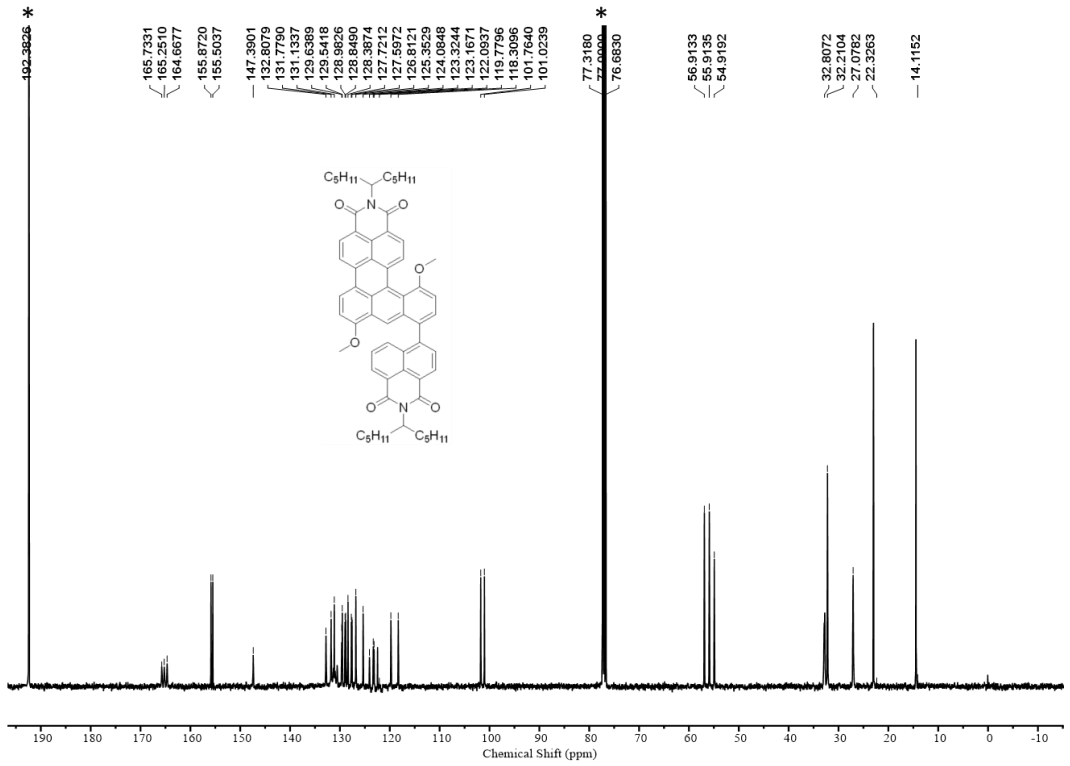

Fig. S20 ^{13}C NMR spectrum (100 MHz) of compound **4** in $CDCl_3/CS_2$ (5/1) at 298 K. (∗ Solvent Peak)

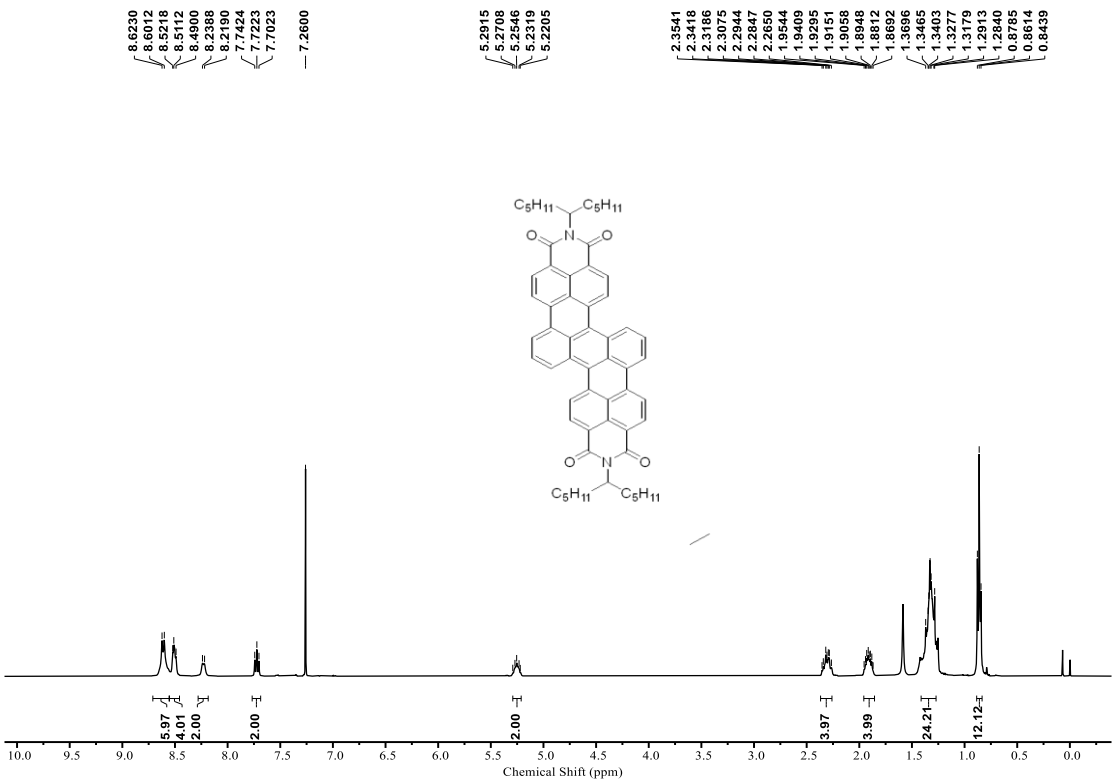

Fig. S21 ^{1}H NMR spectrum (400 MHz) of compound **ADA** in $CDCl_3$ at 298 K.

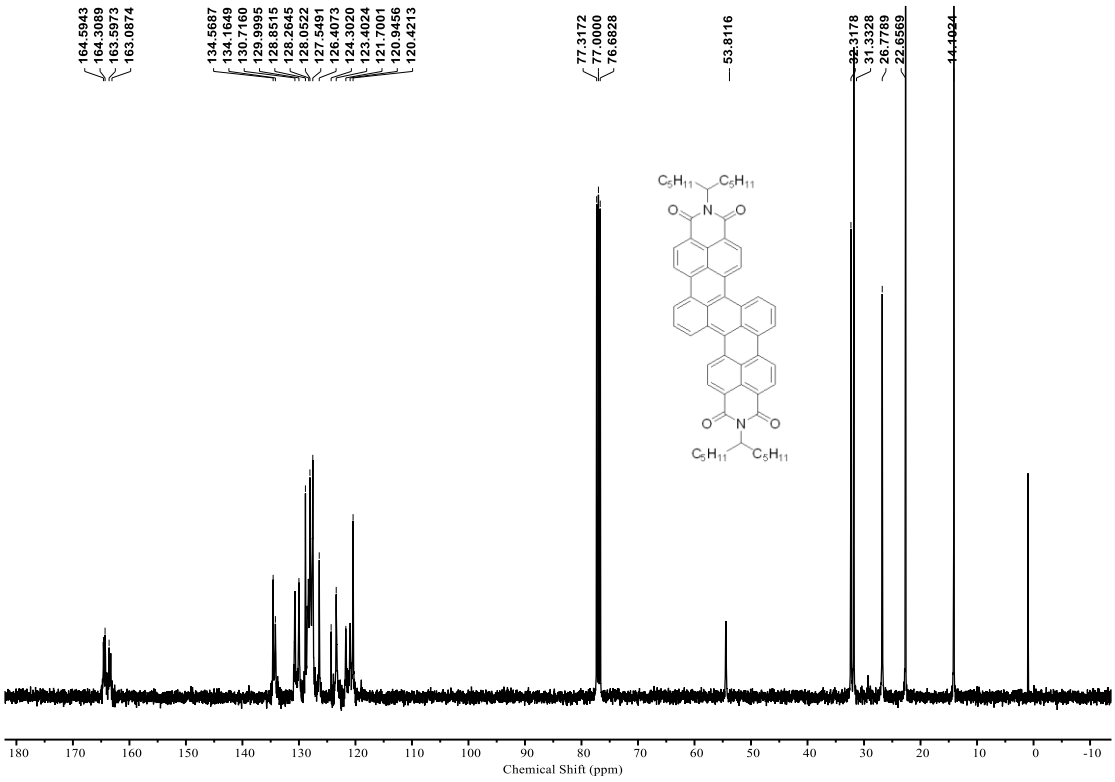

Fig. S22 ^{13}C NMR spectrum (100 MHz) of compound **ADA** in $CDCl_3$ at 298 K.

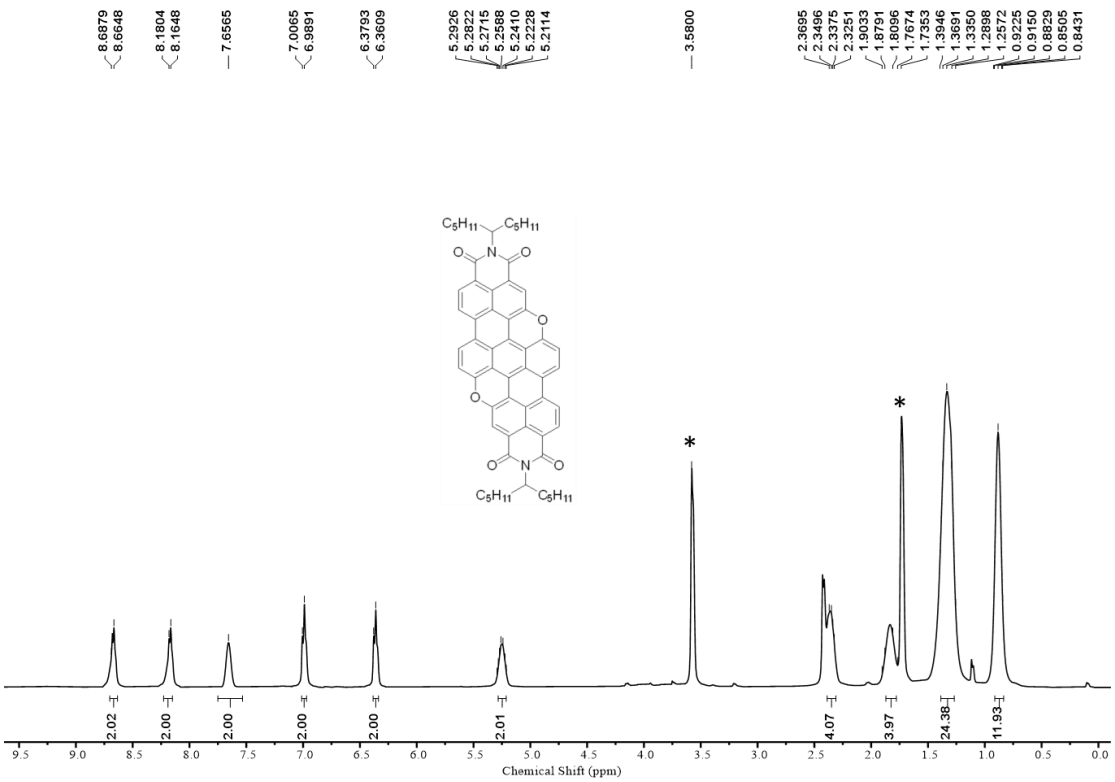

Fig. S23 ^{1}H NMR spectrum (400 MHz) of compound ***O*-ADA** in THF-d_8/CS_2 (5/1) at 298 K. (∗ Solvent Peak)

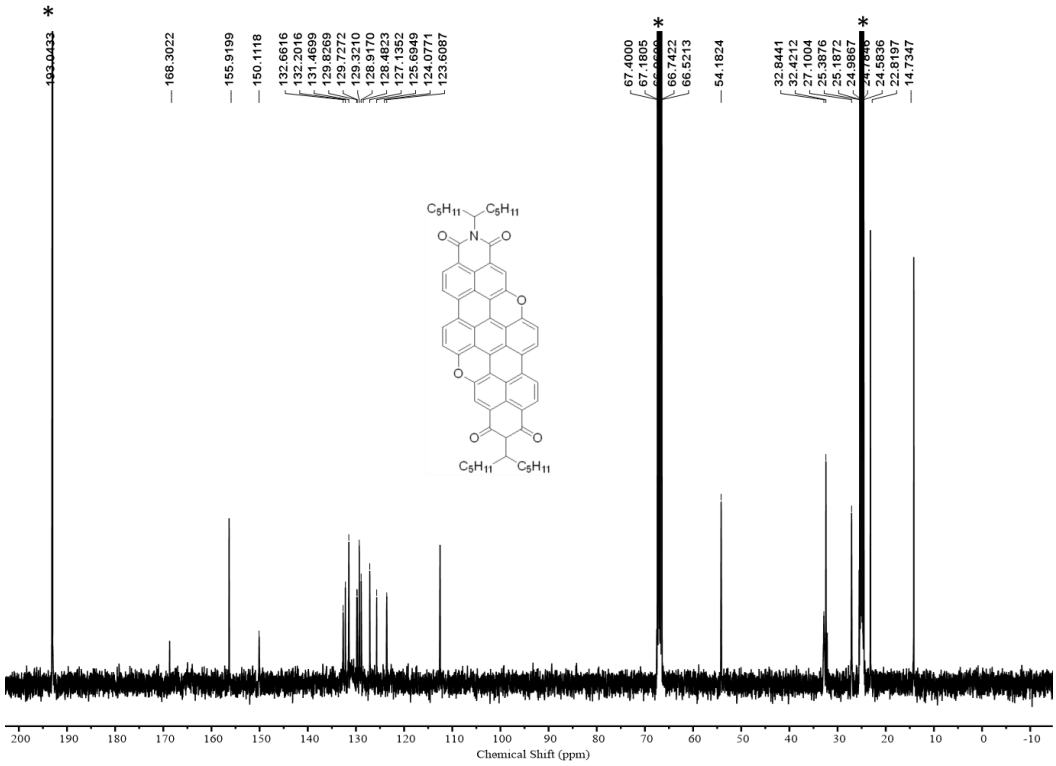

Fig. S24 ^{13}C NMR spectrum (100 MHz) of compound ***O*-ADA** in THF-d_8/CS_2 (5/1) at 298 K. (∗ Solvent Peak)

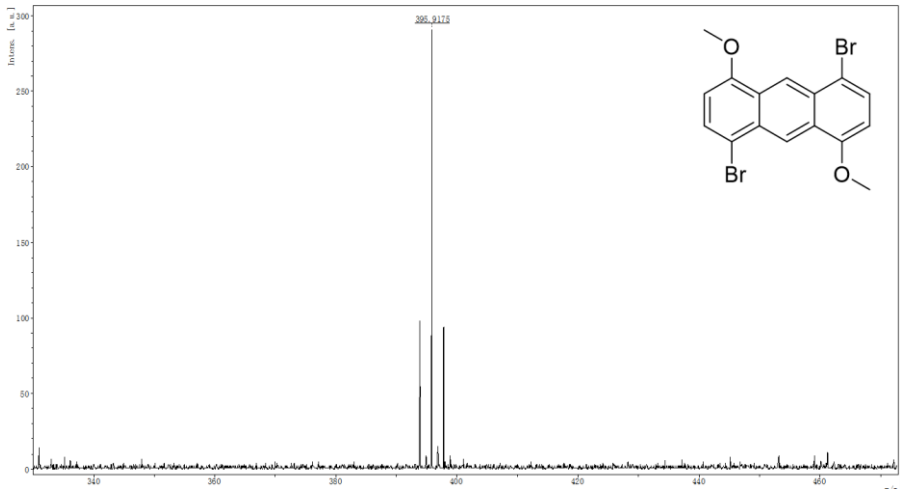

Fig. S25 HR (MALDI-TOF) mass spectrum of compound **1b.**

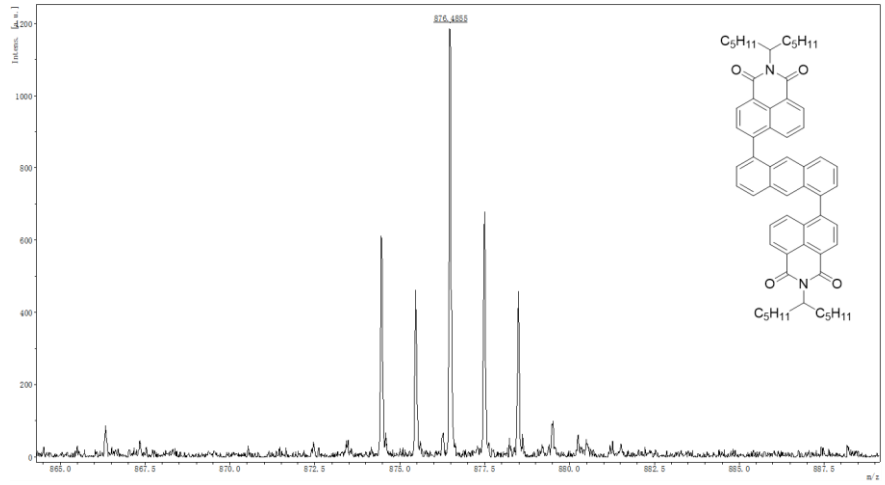

Fig. S26 HR (MALDI-TOF) mass spectrum of compound **2a.**

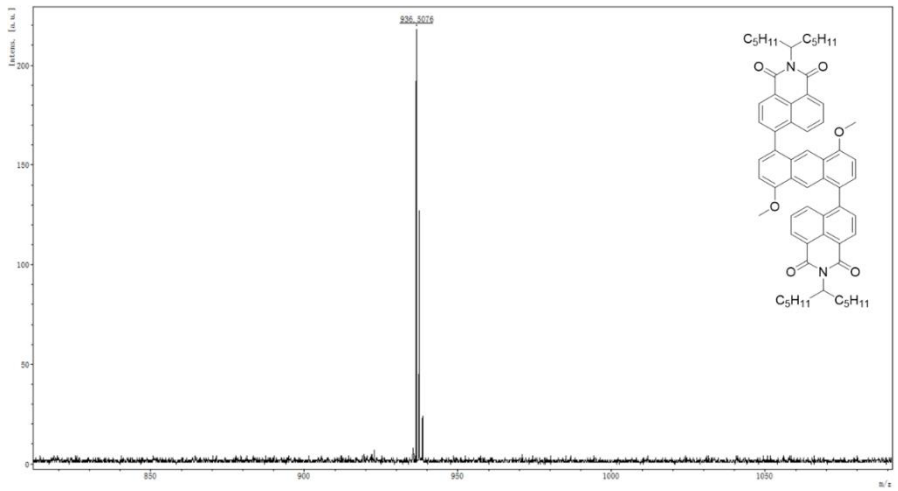

Fig. S27 HR (MALDI-TOF) mass spectrum of compound **2b.**

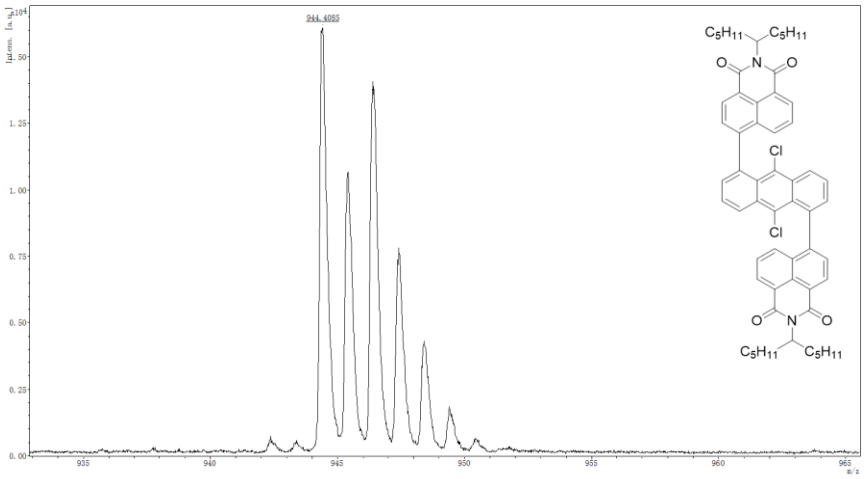

Fig. S28 HR (MALDI-TOF) mass spectrum of compound **3.**

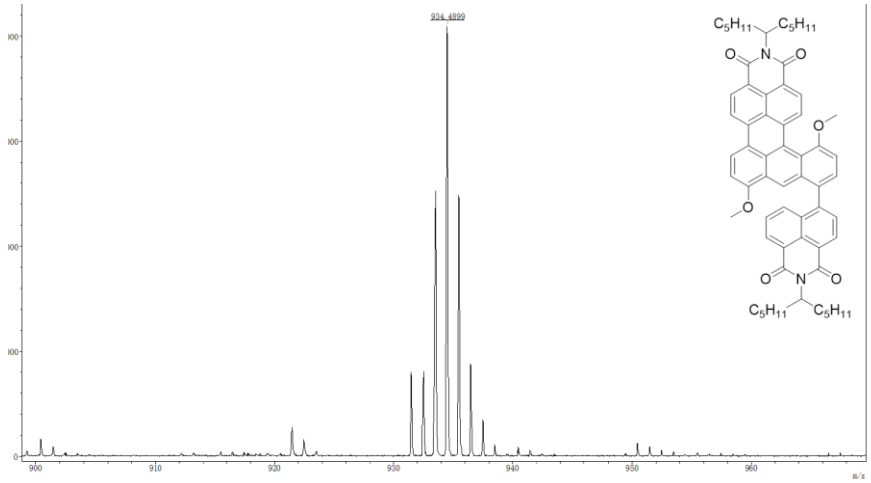

Fig. S29 HR (MALDI-TOF) mass spectrum of compound **4.**

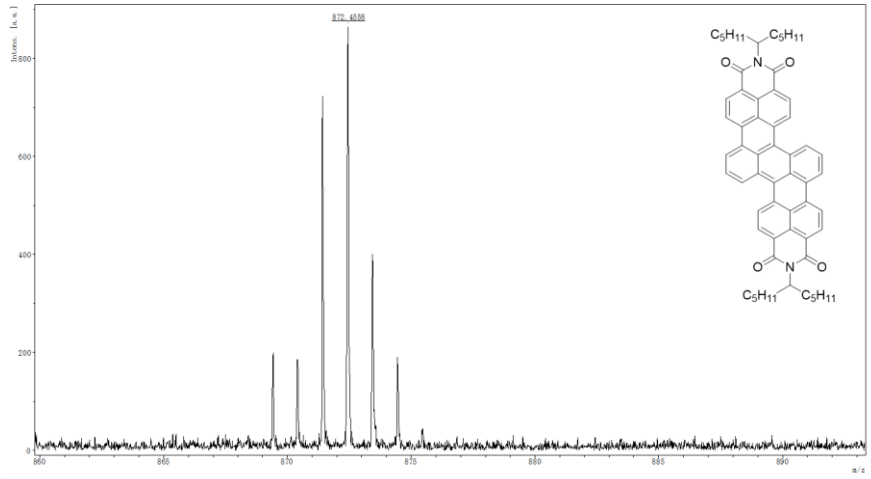

Fig. S30 HR (MALDI-TOF) mass spectrum of compound **ADA.**

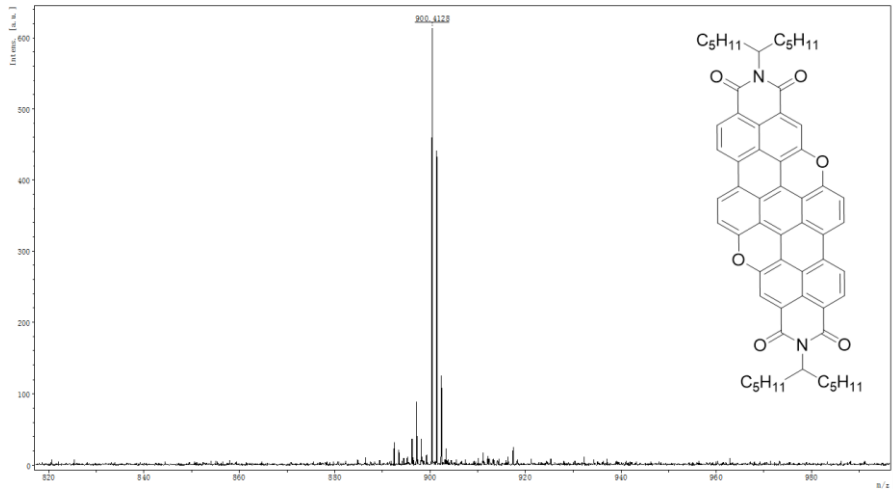

Fig. S31 HR (MALDI-TOF) mass spectrum of compound ***O*-ADA.**

References

1. P. Lynch, L. O'Neill, D. Bradley, H. Byrne, and M. McNamara, *Macromolecules*, 2007, **40**, 7895.
2. (a) M. Feofanov, V. Akhmetov, D. Sharapa and K. Amsharov, *Org. Lett.*, 2020, **22**, 1698; (b) Y. Wang, B. Liu, C. Koh, X. Zhou, H. Sun, J. Yu, K. Yang, H. Wang, Q. Liao, H. Woo and X. Guo, *Adv. Energy Mater.*, 2019, **9**, 1803976.
3. S. Manning, W. Bogen, and L. Kelly, *J. Org. Chem*., 2011, **76**, 6007.
4. (a) C. S. Sample, E. Goto, N. V. Handa, Z. A. Page, Y. Luo and C. J. Hawker, *J. Mater. Chem. C*., 2017, **5**, 1052; (b) Y. Avlasevich and K. Mullen, *Chem. Commun.*, 2006, **42**, 4440.
5. (a) F. Nolde, W. Pisula, S. Muller, C. Kohl, and K. Mullen, *Chem. Mater.*, 2006, **18**, 3715; (b) E. Margulies, J. Logsdon, C. Miller, L. Ma, E. Simonoff, R. Young, G. Schatz, and M. Wasielewski, *J. Am. Chem. Soc*., 2017, **139**, 663; (c) N. Xie, C. Li, J. Liu, W. Gong, B. Z. Tang, G. Li and M. Zhu, *Chem. Commun.*, 2016, **52**, 5808; (d) L. Đorđevic, D. Milano, N. Demitri, and D. Bonifazi, *Org. Lett.*, 2020, **22**, 4283; (e) T. Kamei, M. Uryu, and T. Shimada, *Org. Lett.*, 2017, **19**, 2714; (f) T. Miletic´, A. Fermi, I. Orfanos, A. Avramopoulos, F. Leo, N. Demitri, G. Bergamini, P. Ceroni, M. Papadopoulos, S. Couris, and D. Bonifazi, *Chem. Eur. J.*, 2017, **23**, 2363.